Monthly Notices
of the
ROYAL ASTRONOMICAL SOCIETY
MNRAS **443,** 3809–3818 (2014) doi:10.1093/mnras/stu1406

MaGICC baryon cycle: the enrichment history of simulated disc galaxies

C. B. Brook,[1⋆] G. Stinson,[2] B. K. Gibson,[3,4] S. Shen,[5] A. V. Macciò,[2] A. Obreja,[1] J. Wadsley[6] and T. Quinn[7]

[1]*Departamento de Física Teórica, Universidad Autónoma de Madrid, E-28049 Cantoblanco, Madrid, Spain*
[2]*Max-Planck-Institut für Astronomie, Königstuhl 17, D-69117 Heidelberg, Germany*
[3]*Jeremiah Horrocks Institute, University of Central Lancashire, Preston PR1 2HE, UK*
[4]*Department of Astronomy & Astrophysics, University of California, 1156 High Street, Santa Cruz, CA 95064, USA*
[5]*Institute for Computational Astrophysics and Department of Astronomy & Astrophysics, Saint Mary's University, Halifax, NS B3H 3C3, Canada*
[6]*Department of Physics & Astronomy, McMaster University, Hamilton, Ontario, L8S 4M1, Canada*
[7]*Astronomy Department, University of Washington, Box 351580, Seattle, WA 98195-1580, USA*

Accepted 2014 July 9. Received 2014 July 8; in original form 2013 March 11

ABSTRACT

Using cosmological galaxy formation simulations from the MaGICC (Making Galaxies in a Cosmological Context) project, spanning stellar mass from $\sim 10^7$ to 3×10^{10} $M_\odot$, we trace the baryonic cycle of infalling gas from the virial radius through to its eventual participation in the star formation process. An emphasis is placed upon the temporal history of chemical enrichment during its passage through the corona and circumgalactic medium. We derive the distributions of time between gas crossing the virial radius and being accreted to the star-forming region (which allows for mixing within the corona), as well as the time between gas being accreted to the star-forming region and then ultimately forming stars (which allows for mixing within the disc). Significant numbers of stars are formed from gas that cycles back through the hot halo after first accreting to the star-forming region. Gas entering high-mass galaxies is pre-enriched in low-mass proto-galaxies prior to entering the virial radius of the central progenitor, with only small amounts of primordial gas accreted, even at high redshift ($z \sim 5$). After entering the virial radius, significant further enrichment occurs prior to the accretion of the gas to the star-forming region, with gas that is feeding the star-forming region surpassing 0.1 $Z_\odot$ by $z = 0$. Mixing with halo gas, itself enriched via galactic fountains, is thus crucial in determining the metallicity at which gas is accreted to the disc. The lowest mass simulated galaxy ($M_{\rm vir} \sim 2 \times 10^{10}$ $M_\odot$, with $M_\star \sim 10^7$ $M_\odot$), by contrast, accretes primordial gas through the virial radius and on to the disc, throughout its history. Much like the case for classical analytical solutions to the so-called 'G-dwarf problem', overproduction of low-metallicity stars is ameliorated by the interplay between the time of accretion on to the disc and the subsequent involvement in star formation – i.e. due to the inefficiency of star formation. Finally, gas outflow/metal removal rates from star-forming regions as a function of galactic mass are presented.

Key words: galaxies: evolution – galaxies: formation – galaxies: spiral.

1 INTRODUCTION

The formation, accretion, and expulsion of metals leave important chemical imprints within the stellar and gas-phase components of galaxies. These signatures, including, for example, abundance ratios, metallicity distribution functions (MDFs), and spatially resolved abundance gradients, can be used to constrain the baryonic cycle within galaxies – that is, the infall of gas into a system, its involvement in star formation, and its potential outflow via energy- and/or momentum-driven winds. This cycle, and how it is affected by the mass, environment, and accretion history of the host halo in which a galaxy resides, lies at the heart of galaxy formation.

Chemical evolution models follow the creation and evolution of metals, accounting for the accretion of pristine and pre-enriched gas at rates that are constrained in order to match the observed

⋆E-mail: cbabrook@gmail.com

chemical abundance properties of galaxies (e.g. Timmes, Woosley & Weaver 1995; Gibson 1997; Chiappini, Matteucci & Romano 2001; Fenner & Gibson 2003), as well as properties such as luminosities, star formation rates, and colours. Whilst providing important insights, such models lack the dynamical/kinematic information required for a more comprehensive model of galaxy formation. Models such as Samland, Hensler & Theis (1997) incorporate chemical evolution into a dynamical model of the galaxy, including the mixing of metals in the interstellar medium (ISM), and in the case of Samland & Gerhard (2003), within a growing dark matter halo. One way that chemical evolution modelling can incorporate the full merging and mass evolution history within a cosmological context is via semi-analytic models. Gas accretion and, therefore, star formation, are tied to the growth and merging histories of dark matter haloes, thereby allowing chemical enrichment to be traced (e.g. Calura & Menci 2009; Arrigoni et al. 2010). See Benson (2010) for a review of various ways of modelling galaxy formation, and their advantages and disadvantages.

An even more self-consistent framework can be constructed by embedding star formation, feedback, and chemical enrichment within fully cosmological hydrodynamical simulations of galaxy formation. Indeed, there is a rich vein of literature linking chemical evolution and hydrodynamics in such a manner (e.g. Steinmetz & Mueller 1994; Berczik 1999; Kawata & Gibson 2003; Springel & Hernquist 2003; Bailin et al. 2005; Renda et al. 2005; Martínez-Serrano et al. 2008; Sawala et al. 2010; Kobayashi & Nakasato 2011; Few et al. 2012; Tissera, White & Scannapieco 2012).

However, simulations on cosmological scales cannot resolve the complex processes occurring within a multiphase ISM, where the volume is dominated by hot, diffuse gas while most of the mass lies in cold, dense clouds. Several methods of modelling the ISM within the sub-grid have been developed. Hultman & Pharasyn (1999) used hot and cold phases, and allowed them to interact through radiative cooling and evaporation of the cold clouds. Pearce et al. (2001) set temperature boundaries to decouple cold and hot phases. Springel & Hernquist (2003) developed an analytic model for the sub-grid scale, regulating star formation in a multiphase ISM within a simulation particle. Semelin & Combes (2002) consider a warm gas phase, treated as a continuous fluid using smoothed particle hydrodynamics (SPH), and a cold gas phase, treated by a low-dissipation sticky particle component. Harfst, Theis & Hensler (2006) also used a multiphase ISM, including condensation, evaporation, drag, and energy dissipation, and a star formation efficiency that is dependent on the ISM properties. Scannapieco et al. (2006, see also Marri & White 2003) include a scheme whereby particles with different thermodynamic properties do not see each other as neighbours, allowing hot, diffuse gas to coexist with cold, dense gas. Pelupessy, Papadopoulos & van der Werf (2006) formulate a sub-grid model for gas clouds that use cloud scaling relations, and tracks the formation of H2 on dust grains and its destruction by ultraviolet (UV) irradiation, including the shielding by dust and H2 self-shielding, as well as its collisional destruction in the warm neutral medium. Thacker & Couchman (2001) disallowed radiative losses for 30 Myr from particles which had just been heated by supernovae (SNe), with hot and cold gas coexisting on larger scales, and allowing a wind to develop. Stinson et al. (2006) developed this model further by using the blast-wave model for SNe (McKee & Ostriker 1977) to relate the time-scale of the 'adiabatic' phase to the local density and pressure of the star-forming region.

Within our Making Galaxies in a Cosmological Context (MaGICC) project, we have simulated a suite of galaxies using the cosmological hydrodynamical galaxy formation code GASOLINE, and included blast-wave SN feedback, as well as ionizing feedback from massive stars prior to their explosion as SNe. As discussed in our earlier work, these MaGICC galaxies have the star formation and feedback parameters (see Section 2) tuned to match the stellar mass–halo mass relation. The simulations then match a wide range of galaxy scaling relations (Brook et al. 2012b), over a stellar mass ranging from 2.3×10^8 to 3×10^{10} $M_\odot$ (Table 1). Further, the simulations expel sufficient metals to match local observations (Prochaska et al. 2011; Tumlinson et al. 2011) of O VI in the circumgalactic medium (Brook et al. 2012c; Stinson et al. 2012), and have been shown to match the *evolution* of the stellar mass–halo mass relation (Stinson et al. 2013b; Kannan et al. 2014), as derived in abundance matching studies (Moster, Naab & White 2013).

We showed in Pilkington et al. (2012), and return to below, that our MaGICC simulations do not suffer from any 'G-dwarf problem' – i.e. an overproduction of low-metallicity stars relative to the number observed in nature. Further constraints on our simulations are provided by the so-called 'near-field cosmology': our simulations have appropriately low-mass stellar haloes for their mass and morphological type (see Brook et al. 2004), and abundance ratios which mimic those found in the Milky Way thick and thin discs (Brook et al. 2012c; Stinson et al. 2013a).

This confluence of simulations with observations places necessary constraints on the particular baryon cycle, a cycle which can be measured directly within simulations. What we wonder is, for models that match a range of $z = 0$ relations (see also McCarthy et al. 2012; Aumer et al. 2013, which match at least a sub-set of the relations matched by our simulations), how many degeneracies in the baryon cycle are possible? If a fundamentally different feedback implementation also matches $z = 0$ observations, can it have totally different baryon cycle from ours? By providing quantitative measures of this cycle, we aim to facilitate comparisons with other models, particularly those employing significantly different implementations of star formation and feedback processes, as well as providing predictions for observers.

Previously, Shen, Wadsley & Stinson (2010) showed that in a Milky Way-analogue simulation, intergalactic medium (IGM) metals primarily reside in the so-called warm–hot intergalactic medium (WHIM) with metallicities lying between 0.01 and 0.1 solar with a slight decrease at lower redshifts. In galaxies of such mass, enrichment of the WHIM by proto-galaxies at high redshift means that the majority of gas is pre-enriched prior to accretion to the central galaxy.

Here, we track the baryon cycle of MaGICC galaxies which span more than three orders of magnitude in stellar mass, and present the inflow and outflow rates of their gas and metals. We show the importance of (a) pre-enrichment, and give an indication of the mass range at which it becomes important, and link it to the existence of an accreted stellar halo, (b) enrichment through gas mixing within the halo itself, both during the first accretion to the disc and during galactic fountain cycles, and (c) enrichment within the disc region itself. First, we present the details of the code GASOLINE and the properties of the simulated galaxies in Section 2. In Section 3.1, we explore the evolution of the inflow rates through the virial radius $R_{\rm vir}$, and into the star-forming regions (through $R_{\rm vir}/8$[1]), and the metallicities of such inflowing gas. In Sections 3.2 and 3.4, we

[1] This value is somewhat arbitrary, but is generally a reasonable indication of the region where star formation occurs.

Table 1. Simulation data where gas part is the initial gas particle mass, $c_\star$ is the star formation efficiency parameter, $C_{\rm Diff}$ is the diffusion co-efficient, $M_\star$ and $M_{\rm halo}$ are measured within the virial radius, M_R is the R-band magnitude calculated using SUNRISE, $R_{\rm vir}$ is at 390 times the cosmic background matter density, *acc.* is the fraction of the universal baryon fraction that accrete to $R_{\rm vir}$ during the simulation, while $z = 0$ shows the fraction remaining within $R_{\rm vir}$ at the final timestep, *prim. frac* is the fraction of gas that accretes to $R_{\rm vir}$ that is primordial, and *fount. frac.* is the fraction of stars forming from gas that was cycled through the galactic fountain, requiring that the gas is expelled beyond $R_{\rm vir}/8$ and subsequently re-accreted to the star-forming region.

Name	MUGS label	Gas part. ($M_\odot$)	$c_\star$	$C_{\rm Diff}$	$M_{\rm halo}$ ($M_\odot$)	$R_{\rm vir}$ (kpc)	$M_\star$ ($M_\odot$)	$M_{\rm gas}$ ($M_\odot$)	M_R	Baryon frac. acc.	Baryon frac. $z = 0$	$R_{\rm vir/8}$ acc.	Prim. frac.	Fount. frac.
dG3	15784	3.1×10^3	0.017	0.05	2.2×10^{10}	77	8.9×10^6	4.4×10^8	−12.8	0.46	0.15	0.14	0.95	0.22
SG1	5664	2.5×10^4	0.017	0.05	6.5×10^{10}	115	2.3×10^8	4.7×10^9	−17.0	0.85	0.50	0.55	0.62	0.37
SG2	1536	2.5×10^4	0.017	0.05	8.3×10^{10}	125	4.5×10^8	6.2×10^9	−17.5	1.0	0.52	0.66	0.57	0.39
SG3	15784	2.5×10^4	0.017	0.05	1.8×10^{11}	162	4.2×10^9	1.5×10^{10}	−20.0	1.0	0.73	0.78	0.53	0.32
$SG3_{LD}$	15784	2.5×10^4	0.017	0.01	1.8×10^{11}	163	3.7×10^9	1.7×10^{10}	−19.8	1.0	0.76	0.77	0.57	0.32
SG4	15807	2.5×10^4	0.017	0.05	3.2×10^{11}	190	1.4×10^{10}	2.8×10^{10}	−21.2	1.0	0.85	0.80	0.50	0.32
L*G2	1536	2.0×10^5	0.033	0.05	7.6×10^{11}	257	3.0×10^{10}	6.6×10^{10}	−21.7	1.0	0.82	0.69	0.08	0.18
L^*G2_{LD}	1536	2.0×10^5	0.033	0.01	7.6×10^{11}	258	2.7×10^{10}	7.1×10^{10}	−21.6	1.0	0.87	0.69	0.22	0.18

provide the time-scales of gas entering the virial radius, entering the star-forming region, cycling though the galactic fountain, and finally forming stars. In Section 3.5, we examine the evolution of the rates of outflow from the star-forming regions (through $R_{\rm vir}/8$) and their metallicities. We end by discussing our results and their implications in Section 4.

2 THE SIMULATIONS

The MaGICC simulations were realized using GASOLINE (Wadsley, Stadel & Quinn 2004), a fully parallel, gravitational N-body + SPH code. Cooling via hydrogen, helium, and various metal lines is included, after Shen et al. (2010), employing CLOUDY (v.07.02; Ferland et al. 1998), assuming ionization equilibrium and cooling rates self-consistently, in the presence of a uniform UV ionizing background (Haardt & Madau 1996).

We do not follow the atomic-to-molecular transition. Simulations of dwarf galaxies with H2- regulated star formation and comparable resolution to our low-mass galaxies have been run to $z = 0$ by Christensen et al. (2012). However, the resolution of our most massive galaxies precludes the inclusion of such processes. We prevent gas from collapsing to higher densities than SPH can physically resolve: (i) pressure is added to the gas in high-density star-forming regions (Robertson & Kravtsov 2008), to ensure that gas resolves the Jeans mass and does not artificially fragment, and (ii) a maximum density limit is imposed by setting a minimum SPH smoothing length of 0.25 times that of the gravitational softening length.

The simulations described here are cosmological zoom simulations derived from the McMaster Unbiased Galaxy Simulations (MUGS; Stinson et al. 2010), which use *Wilkinson Microwave Anisotropy Probe* 3 (*WMAP*3) cosmology (Spergel et al. 2007) and follow evolution from $z = 99$ to 0. For SG1 to SG4 (see Table 1), the initial conditions are 'scaled-down' variants of those employed in the original MUGS work, so that rather than residing in a 68 Mpc cube, they lie within a cube with 34 Mpc sides (and for dG3, they are scaled down further to a cube with 17 Mpc sides). This resizing allows us to compare galaxies with exactly the same merger histories at a variety of masses. Differences in the underlying power spectrum that result from this rescaling are minor (Macciò, Dutton & van den Bosch 2008; Springel et al. 2008; Kannan et al. 2012), and do not significantly affect our results. Certainly, if a statistical sample were being examined, this rescaling may be important, but for the purposes of this study, only small quantitative differences would eventuate.

2.1 Star formation and feedback

All simulations use the feedback scheme as described in Stinson et al. (2012, 2013b), which we describe briefly here. Gas is eligible to form stars when it reaches cool temperatures ($T < 15\,000$ K) in a dense environment ($n_{\rm th} > 9.3$ cm^{-3}); the latter is set to be the maximum density that gas can reach using gravity – i.e. $32\,m_{\rm gas}/\epsilon^3$. We note that in all our simulations, stars form at temperatures significantly below the threshold temperature, meaning that it is the threshold density that is critical in determining whether gas is eligible for star formation. Such gas is converted to stars according to a Schmidt law:

$$\frac{\Delta M_\star}{\Delta t} = c_\star \frac{m_{\rm gas}}{t_{\rm dyn}}, \quad (1)$$

where $\Delta M_\star$ is the mass of the stars formed in Δt, the time between star formation events (0.8 Myr in these simulations), $m_{\rm gas}$ is the mass of the gas particle, $t_{\rm dyn}$ is the gas particle's dynamical time, and $c_\star$ is the efficiency of star formation, in other words, the fraction of gas that will be converted into stars during $t_{\rm dyn}$. Effective star formation rates are determined by the combination and interplay of $c_\star$ and feedback, and so degeneracies do exist between feedback energy and the value of $c_\star$. In this study, $c_\star$ is ultimately the free parameter that sets the balance of the baryon cycle of cooling gas, star formation, and gas heating.

Two types of feedback from massive stars are considered, SNe and early stellar radiation feedback. SN feedback is implemented using the Stinson et al. (2006) blast-wave formalism, depositing 10^{51} erg into the surrounding ISM at the end of the stellar lifetime of stars more massive than 8 $M_\odot$. Since stars form from dense gas, this energy would be quickly radiated away due to the efficient cooling; for this reason, cooling is disabled for particles inside the blast region. Metals are ejected from Type II supernovae (SNeII), Type Ia supernovae (SNeIa), and the stellar winds driven from asymptotic giant branch (AGB) stars, and distributed to the nearest gas particles using the smoothing kernel (Stinson et al. 2006), adopting literature yields for SNeII (Woosley & Weaver 1995), SNeIa (Nomoto et al. 1997), and AGB stars (van den Hoek & Groenewegen 1997). We trace the lifetimes of stars and SNe and trace elements Fe, O, C, N, Ne, Si, Mg, depositing those metals formed at each timestep into the neighbouring gas particles.

Metal diffusion is included, allowing proximate gas particles to mix their metals, by treating unresolved turbulent mixing as a shear-dependent diffusion term (Shen et al. 2010). Metal cooling is

calculated based on the diffused metals. The impact on the structure of resulting simulated ISM was explored by Pilkington et al. (2011).

Radiation energy feedback from massive stars has been included in our simulations. To model the luminosity of stars, a simple fit of the mass–luminosity relationship observed in binary star systems by Torres (2010) is used:

$$\frac{L}{\mathrm{L}_\odot} = \begin{cases} \left(\frac{M}{\mathrm{M}_\odot}\right)^4, & M < 10\,\mathrm{M}_\odot \\ 100\left(\frac{M}{\mathrm{M}_\odot}\right)^2, & M > 10\,\mathrm{M}_\odot. \end{cases} \quad (2)$$

Typically, this relationship leads to 2×10^{50} erg of energy being released from the high-mass stars per $\mathrm{M}_\odot$ of the entire stellar population over the ∼4.5 Myr between a star's formation and the commencement of SNeII in the region. These photons do not couple efficiently with the surrounding ISM (Freyer, Hensler & Yorke 2006). To mimic this highly inefficient energy coupling, we inject 10 per cent of the energy as thermal energy in the surrounding gas, and cooling is *not* turned off. Such thermal energy injection is highly inefficient at the spatial and temporal resolution of cosmological simulations (Katz 1992; Kay et al. 2002), as the characteristic cooling time-scales in the star-forming regions are lower than the dynamical time. Over 90 per cent is typically radiated away within a single dynamical time, meaning that our effective efficiency of coupling radiation energy feedback to the ISM is ∼1 per cent.

As with other galaxy formation simulations in the literature, galaxy properties are not precisely the same at different resolutions when the same parameters are used (e.g. Scannapieco et al. 2012). We aim to retain the same baryon cycle at the different resolutions as this drives the simulated galaxy properties. To achieve this, we adjusted our free parameter $c_\star$, in order to ensure that each galaxy matches the $M_\star$–$M_{\rm halo}$ relation at $z = 0$ (Moster et al. 2010).

2.2 Turbulent metal diffusion

Galactic inflows and outflows should be turbulent and thus mixing is essential for IGM studies. SPH does not implicitly include diffusion of scalar quantities such as metals, resulting in physically incorrect consequences (e.g. Wadsley, Veeravalli & Couchman 2008; Shen, Wadsley & Stinson 2010; Pilkington et al. 2012). By contrast, Eulerian grid codes mix due to the necessary advection estimates (e.g. Few et al. 2012). To generate similar non-radiative galaxy cluster entropy profiles with SPH as with high-resolution grid codes, Wadsley et al. (2008) include a diffusion coefficient, $D = C_{\rm Diff}\Delta v h_{\rm SPH}$, based on the pairwise velocity, Δv, at the resolution scale, $h_{\rm SPH}$. A coefficient value of the order of 0.05–0.1 is expected from turbulence theory (depending on the effective measurement scale, h). A conservative choice of $C_{\rm Diff} = 0.05$ was sufficient to match the cluster comparison (Wadsley et al. 2008), solving a major discrepancy between SPH and grid codes (Frenk et al. 1999). A similar scheme has been applied to SN remnants (Greif et al. 2009).

GASOLINE now uses a more robust mixing estimator (Shen et al. 2010), similar to that proposed by Smagorinsky (1963) for the atmospheric boundary layer. Rather than simply using velocity differences (Wadsley et al. 2008; Greif et al. 2009), the diffusion coefficient is now calculated according to a turbulent mixing model:

$$\begin{aligned} \frac{\mathrm{d}A}{\mathrm{d}t}|_{\rm Diff} &= \nabla(D\nabla A), \\ D &= C_{\rm Diff}\,|S_{ij}|\,h^2, \end{aligned} \quad (3)$$

where A is any scalar. The diffusion expression for a scalar A_p on particle p is computed as

$$\begin{aligned} \tilde{S}_{ij}|_p &= \frac{1}{\rho_p}\sum_q m_q(v_j|_q - v_j|_p)\nabla_{p,i}W_{pq}, \\ S_{ij}|_p &= \frac{1}{2}(\tilde{S}_{ij}|_p + \tilde{S}_{ji}|_p) - \delta_{ij}\frac{1}{3}\,\mathrm{Trace}\,\tilde{S}|_p, \\ D_p &= C_{\rm Diff}\,|S_{ij}|_p|\,h_p^2, \\ \frac{\mathrm{d}A_p}{\mathrm{d}t}|_{\rm Diff} &= -\sum_q m_q\frac{(D_p + D_q)(A_p - A_q)(\boldsymbol{r}_{pq}\cdot\nabla_p W_{pq})}{\frac{1}{2}(\rho_p + \rho_q)\,\boldsymbol{r}_{pq}^2}, \end{aligned} \quad (4)$$

where the sums are over 32 SPH neighbours, q, δ_{ij} is the Kronecker delta, W is the SPH kernel function, ρ_q is the density, $\boldsymbol{r}_{pq}$ is the vector separation between particles, $v_i|_q$ is the particle velocity component in direction i, ∇_p is the gradient operator for particle p, and $\nabla_{p,i}$ is the ith component of the resultant vector. As the coefficient depends on the velocity shear, it better models the mixing in shearing flows. Where there is no shearing motion between two phases of fluids, such as for compressive or purely rotating flows, no turbulent diffusion is added.

For our fiducial models, we follow the (conservative) choice of Shen et al. (2010), $C_{\rm Diff} = 0.05$. We also run two simulations with significantly lower diffusion, $C_{\rm Diff} = 0.01$, to test whether this diffusion term is driving our results.

3 RESULTS

Table 1 lists the properties of the simulated galaxies, including the mass of gas particles, star formation efficiency ($c_\star$), metal diffusion coefficient ($C_{\rm Diff}$), total halo mass ($M_{\rm halo}$), virial radius ($R_{\rm vir}$), stellar mass ($M_\star$), gas mass ($M_{\rm gas}$), and R-band magnitude (M_R).

We also show in Table 1 the final ($z = 0$) baryon mass fraction, as compared with the universal value of 0.153, and the fraction of baryons that are ever accreted to within the virial radius. In all galaxies with $M_{\rm vir} > 8 \times 10^{10}$, we do not find any indication of prevention of baryons being accreted. Baryons are subsequently ejected from the simulated galaxies, with 50 per cent ejected from SG2 ($M_{\rm vir} = 8.3 \times 10^{10}$ $\mathrm{M}_\odot$), decreasing to 18 per cent of gas ejected for L*G2 ($M_{\rm vir} = 7.8 \times 10^{11}$ $\mathrm{M}_\odot$). In the two lowest mass galaxies, dG3 and SG1, gas is actually prevented from being accreted across $R_{\rm vir}$. In fact, over half the baryons are never detected within the virial radius of the lowest mass galaxy (dG3: $M_{\rm vir} = 2.2 \times 10^{10}$ $\mathrm{M}_\odot$). This is due to a combination of the UV background radiation and the effect of large-scale outflows affecting accreting gas.

We also show the baryon fraction that accretes to the star-forming region: note that we compare to the universal value expected within $R_{\rm vir}$. As is also shown in Table 1, in the lowest mass case, only 14 per cent of the baryons expected within the virial radius actually accrete to the star-forming region. This rises to 78 per cent in SG3 ($M_{\rm vir} = 1.8 \times 10^{11}$ $\mathrm{M}_\odot$) and 80 per cent in SG4 ($M_{\rm vir} = 3.2 \times 10^{11}$ $\mathrm{M}_\odot$), before dropping to 69 per cent in L*G2, possibly due to the shock heating of gas in this most massive galaxy, which is above the critical mass for shock heating (Dekel & Birnboim 2006). Such shock heating occurs in simulations such as ours (Kereš et al. 2005; Brooks et al. 2009).

The inflows and outflows are all self-consistently modelled in our simulations, so the outflows we measure in this section have been affected by the inflows, and the inflows are indeed affected by the outflows. We present here net inflows and outflows, as well as quantifying the recycling through galactic fountains. The direction

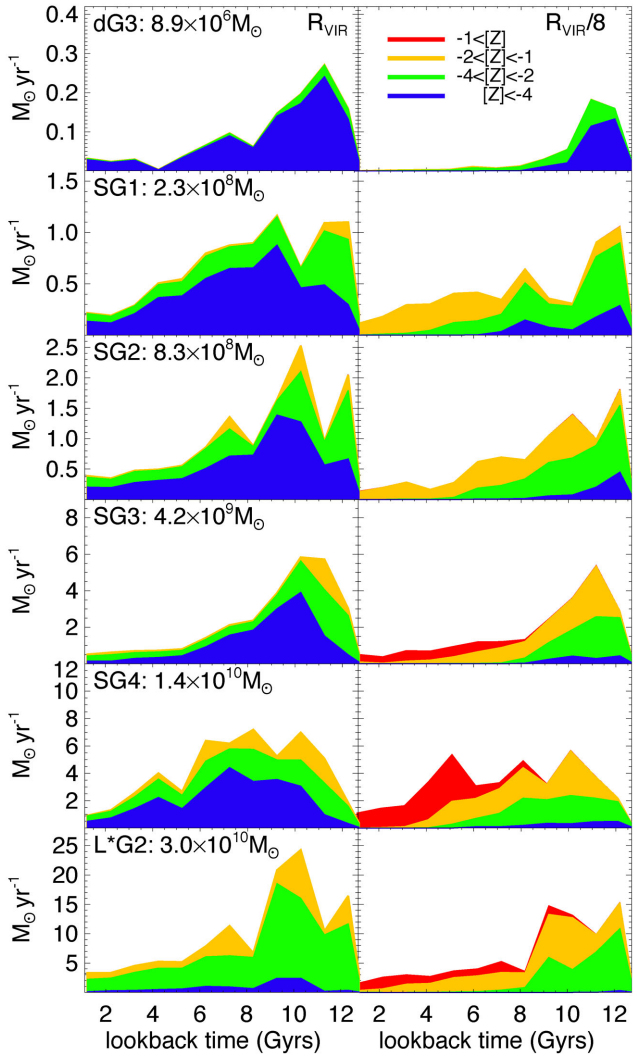

Figure 1. Inflow rates ($M_\odot$ yr^{-1}) of gas entering $R_{\rm vir}$ (left-hand panels) and $R_{\rm vir}/8$ (right-hand panels) for the first time, as a function of time. The rates are broken into four metallicity bins $[Z] < -4$ (blue), $-4 < [Z] < -2$ (green), $-2 < [Z] < -1$ (yellow), and $-1 < [Z]$ (red). The stellar mass at $z = 0$ for each simulated galaxy is shown in the left-hand panels.

of outflows versus inflows in disc galaxies, and its relation to angular momentum, was studied for these simulations in Brook et al. (2011), which showed the preference for outflows to be perpendicular to the disc while inflows are preferentially in the plane of the disc.

3.1 Inflows

In Fig. 1, we show the inflow rates ($M_\odot$ yr^{-1}) of gas entering $R_{\rm vir}$ (left-hand panels) and $R_{\rm vir}/8$ (right-hand panels) for the first time, as a function of time. The rates are broken into four metallicity bins $[Z] < -4$ (blue), $-4 < [Z] < -2$ (green), $-2 < [Z] < -1$ (yellow), and $-1 < [Z]$ (red). $R_{\rm vir}/8$ is used to delineate the star-forming region of the galaxy. Here, we have used $[Z] \equiv \log Z/Z_\odot$.

In the lowest mass case[2] (dG3), primordial gas enters $R_{\rm vir}$ at all times, and most of the gas entering the star-forming region is also primordial. As we move to higher masses, more gas is pre-enriched prior to entering the virial radius of the central galaxy. This pre-enrichment results from the outflows from sub-haloes that have collapsed and formed stars prior to a lookback time of 12.6 Gyr ($z = 5.5$), enriching the IGM from which the central galaxy draws its gas. This finding is consistent with what was found in Shen et al. (2010), who examined a simulation of similar mass as L*G2, with our new study showing that this pre-enrichment is also important in lower mass galaxies, although progressively less so as we move to lower masses. The fraction of primordial gas accreted to the virial radius between lookback times of 12.5 ($z \sim 5.5$) and 10 Gyr ($z \sim 2$) goes from 95 per cent for a simulation with $M_\star = 8.9 \times 10^6$ $M_\odot$ to 8 per cent for $M_\star = 3.0 \times 10^{10}$ $M_\odot$, as shown in Table 1. It is only in the very lowest mass simulation that sub-halo progenitors are too low in mass to form stars, prevented by the ionizing UV background radiation. In all haloes above total mass 2.2×10^{10} $M_\odot$, local collapsing overdensities outside the central galaxy result in sub-halo progenitors that form stars and enrich the IGM during the hierarchical build-up of the galaxies.

Inflow rates peak within ~10–12 Gyr ago ($3 < z < 2$), in all cases except SG4, which has a late merger which brings in significant amounts of gas ~8 Gyr ago ($z \sim 1$).

The most important aspect of Fig. 1 is possibly the differences between the inflows through $R_{\rm vir}$ (left-hand panels) and through $R_{\rm vir}/8$ (right-hand panels). First, not all gas accreted to $R_{\rm vir}$ cools to the star-forming region ($R_{\rm vir}/8$), with values ranging from ~40 per cent in the lowest mass halo to ~70 per cent in the three highest mass cases. The most striking feature though is the difference between the metallicity of gas as it accretes to $R_{\rm vir}$ for the first time and when it accretes to the star-forming region. The metallicity of the gas has been enhanced during its trajectory through the galactic halo, as it mixes with gas that has been enriched in proto-galaxies and by galactic fountains.

Fig. 2 summarizes the metallicity of the baryons as they accrete and subsequently form stars. The MDFs of the stars at $z = 0$ (blue line)[3] are shown along with the MDFs of the gas from which those stars were born, measured when the gas first accreted to the virial radius of the galaxy (red line) and when it first reaches the star-forming region (green line). Gas with $[Z] < -5$ is taken as primordial and is shown in the plots at $[Z] < -5$. Significant amount of primordial gas is accreted to $R_{\rm vir}$ in the low-mass galaxies. Pre-enrichment in non-central proto-galaxies is significant in $L_\star$ galaxies. The metals contained in the gas particles that were not previously within non-central proto-galaxies have come from mixing due to metal diffusion from metals of the gas pre-enriched in proto-galaxies.

3.2 Gas time-scales within the corona and disc

In Fig. 3, we plot as a black line the time taken between crossing the virial radius and accretion to the star-forming region ($t_{\rm Rvir/8} - t_{\rm Rvir}$), for gas which subsequently forms stars. For this star-forming gas, we also plot the time taken between entering the star-forming region and the time of star formation ($t_{\rm form} - t_{\rm Rvir/8}$, red line). Negative values of $t_{\rm form} - t_{\rm Rvir/8}$ indicate accreted stars. It is interesting (if not surprising) that the galaxies that are massive enough to have accreted stars, all accrete pre-enriched gas even as far back as $z = 5.5$, whereas it is only in the lowest mass dwarf galaxy that stellar

[2] The low-mass simulations have higher resolution, and thus our results are not due to an inability to resolve sub-structure.

[3] Note the similarity between the $z = 0$ MDF of SG3 and that of 11mChab from Pilkington et al. (2012); the two simulations differ only in their adopted star formation efficiencies $c_\star$.

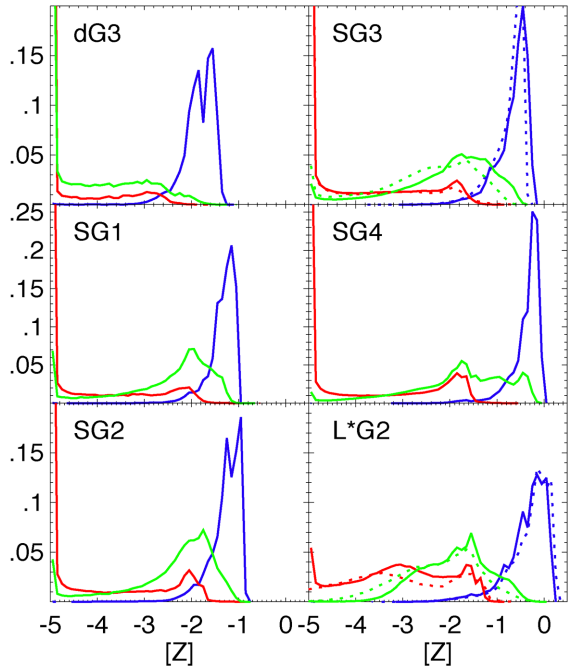

Figure 2. MDFs of stars at $z = 0$ (blue line), along with the MDFs of the gas from which those stars were born, measured when the gas first accreted to the virial radius, $R_{\rm vir}$ of the galaxy (red line), and when it first reaches the star-forming region, $R_{\rm vir}/8$ (green line). Gas with $[Z] < -5$ is shown in the plots at $[Z] = -5$. Significant amount of primordial gas is accreted to ($R_{\rm vir}$) in the low-mass galaxies. Dotted lines in the top-right and bottom-right panels show the minor effect of a five-fold decrease in the metal diffusion coefficient (see Section 3.8).

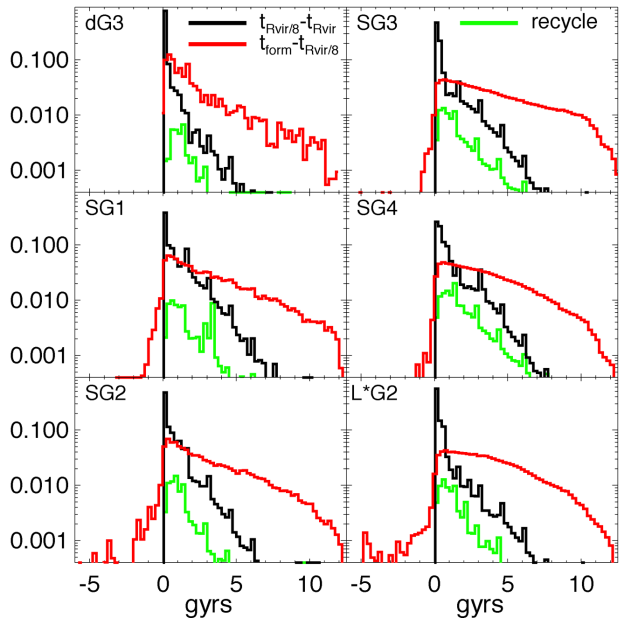

Figure 3. Time taken between crossing the virial radius, $t_{\rm Rvir}$, and accretion to the star-forming region, $t_{\rm Rvir/8}$ (i.e. $t_{\rm Rvir/8} - t_{\rm Rvir}$, black line) for all gas which subsequently forms stars at $t_{\rm form}$. We also show the time taken between accretion to $R_{\rm vir/8}$ and $t_{\rm form}$ ($t_{\rm form} - t_{\rm Rvir/8}$, red line). Negative values of $t_{\rm form} - t_{\rm Rvir/8}$ indicate accreted stars. The green line shows the distributions of times of the galactic fountain cycle for each galaxy – i.e. the time between leaving the star-forming region and being re-accreted to the star-forming region. Each histogram shows the gas mass as a fraction of the total $z = 0$ stellar mass.

accretion does not occur, meaning that the surrounding IGM is not enriched and gas is accreted in a pristine state.

As can be garnered from Fig. 3, gas accretes fairly rapidly from the virial radius to the star-forming region, generally in less than 500 Myr, but with a significant tail out to 5 Gyr. Apparently though, this is long enough for some enrichment to occur. The length of time between gas being accreted to the star-forming region and actually forming stars, is broad, reflecting the low efficiency of star formation in turning gas into stars. This allows gas to enrich significantly and relatively uniformly, which results in the narrow MDFs of the stars, as seen by the blue lines of Fig. 2.

Time-scales can be approximated by simple exponential functions, with the exponent of the time taken between crossing the virial radius and entering the star-forming region ($t_{\rm Rvir/8} - t_{\rm Rvir}$, black line), ranging from $\sim$1 to 1.5 Gyr^{-1}, with mean $\sim$1.2 Gyr^{-1} and no clear discernible trend with mass (at least within our small sample). The exponent of the time taken between accretion to the star-forming region and forming a star (red line) ranges from $\sim$2 to 5 Gyr^{-1}, with mean $\sim$4.3 Gyr^{-1} and some suggestion that lower mass galaxies have a shallower slope, but again a larger statistical sample will be required.

3.3 Accreted stars

As mentioned above, negative values of $t_{\rm form} - t_{\rm Rvir/8}$ in Fig. 3 indicate accreted stars. Few stars accrete directly from sub-haloes, and these generally have low metallicity and make up the low-metallicity tail of the stellar MDF, and mostly end in the low-mass stellar halo. Gas with low metallicity that falls to the disc generally does not form stars straight away (as shown in Fig. 3), so it has higher metallicity (generally) by the time it forms stars. This is why there are few stars with $\log(Z/Z_\odot)$ below -3, in line with observations, i.e. this is the reason why we do not have a g-dwarf problem in these simulations. The simulations do make a small number of stars with $\log(Z/Z_\odot) < -3$.

All simulated galaxies more massive than dG3 clearly show stellar accretion in Fig. 3. The time-scale over which accretion occurs depends on the particular merger history of each galaxy. This is reflected in the fact that SG2 and L*G2 have, by design, the same merger histories and show similarities in the time-scales of star formation for their accreted stars, i.e. the negative values of the red lines of Fig. 3.

3.4 Recycling of gas through the corona

Significant numbers of stars are formed from gas that, subsequent to accretion to the star-forming region, cycles back through the halo in a 'galactic fountain' prior to eventually forming stars. The fraction of star-forming gas involved in galactic fountains, for our simulation suite, is shown in column 13 of Table 1. Although a larger statistical sample may be necessary to fully investigate the dependence on mass, our study indicates a balance where, in the lowest mass galaxy, only 22 per cent of stars form from gas that was involved in a fountain, presumably because outflows tend to be blown further and do not generally re-accrete. At the other end of the mass spectrum (L*G2), gravity inhibits large-scale fountains of gas reaching beyond $R_{\rm vir}/8$, with 18 per cent of stars formed from such gas. It is in intermediate masses where the galactic fountain is most prevalent, with up to 39 per cent of stars forming from gas cycled through a galactic fountain in a galaxy with halo (stellar) mass of 8.3×10^{10} M$_\odot$ (4.5×10^8 M$_\odot$). We note that these fractions are sensitive to the chosen radius.

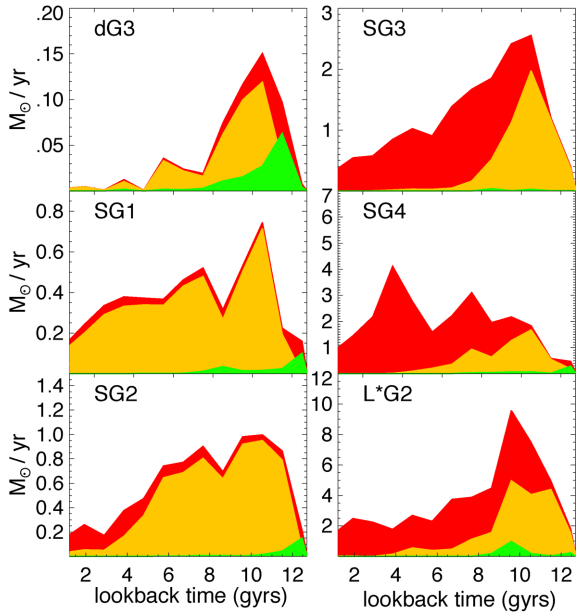

Figure 4. Outflow rates ($M_\odot$ yr^{-1}) of gas through $R_{vir}/8$, as a function of time. The rates are broken up into three metallicity bins: $-4 < [Z] < -2$ (green), $-2 < [Z] < -1$ (yellow), and $-1 < [Z]$ (red).

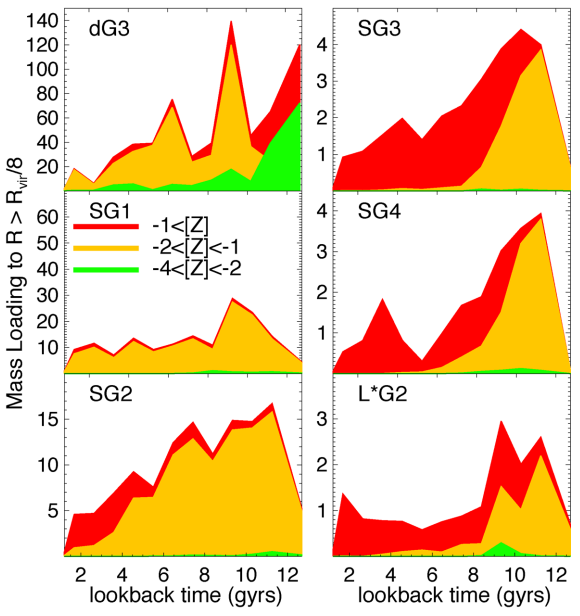

Figure 5. Mass loadings: outflow rates ($M_\odot$ yr^{-1}) of gas through $R_{vir}/8$, divided by the star formation rates, as a function of time. These 'mass loadings' are broken up into three metallicity bins: $-4 < [Z] < -2$ (green), $-2 < [Z] < -1$ (yellow), and $-1 < [Z]$ (red).

We plot, as a green line in Fig. 3, the distributions of times of the galactic fountain cycle for each galaxy – i.e. the time between leaving the star-forming region and being re-accreted to the star-forming region. In each case, this has a similar distribution to the time-scale for accreting from the virial radius to the star-forming region.

The recycle time-scales can be loosely fitted by exponentials which have exponents within 15 per cent of those of the time taken from the virial radius to the star-forming region, ranging from ~ -1 to -1.7 Gyr^{-1}, with a mean of ~ -1.3 Gyr^{-1}. Somewhat surprisingly, the time-scales of the galactic fountains do not show any strong trend with galaxy mass.

We are not able to resolve the interaction between clouds of fountain gas and the hot corona with the same detail as e.g. Marinacci et al. (2010), where lower metallicity coronal gas becomes entrained with the fountain gas, and thus the inflowing fountain gas has lower metallicity than the outflows. We have simply traced the gas particles which flow out of, and back into, the star-forming region, whilst any gas swept up in this fountain would simply have been included within our accounting of inflowing gas. We do note, however, that the re-accreted gas particles experience a small loss of metals due to metal diffusion during this cycle, indicating that they are mixing with the lower metallicity halo gas through the fountain.

3.5 Outflows

To what degree are metals removed from the star-forming region during a galaxy's evolution? In Fig. 4, we show the outflow rates ($M_\odot$ yr^{-1}) of gas from the star-forming region – i.e. outflow rates through $R_{vir}/8$, as a function of time, corresponding to the amount of metals blown into regions that allow pollution of the infalling gas. The rates are broken up into three metallicity bins: $[Z] < -4$ (blue), $-4 < [Z] < -2$ (green), and $-2 < [Z] < -1$ (yellow). Outflows are significantly enriched with metals, and are enriching the interstellar, cirumgalactic, and intergalactic media.

3.6 Mass loading

We can also plot the outflows in terms of the mass loading factor in Fig. 5 , which measures outflow rates compared to the star formation rates. First, we note again that outflow rates *are* sensitive to the radius through which one measures outflows: in Brook et al. (2012a), we showed that the distribution of distances that outflowing gas travels from the star-forming region drops off exponentially. We are interested in the outflows from the star-forming region, as this is what helps determine the availability of gas and metals for subsequent star formation. We therefore have measured the mass loading by determining outflows rates through $R_{vir}/8$.

As can be seen, the mass loading factors for the lowest mass galaxies are high, with gas outflowing from the star-forming region at rates that are factors of 100 greater than the star formation rates at high redshift. Mass loadings are galaxy mass dependent and redshift dependent, with the highest mass loadings occurring in the lowest mass galaxies at high redshift. The highest mass simulation, the L* galaxy, has had gas outflows from the star-forming region at rates similar to the star formation rate since $z \sim 1$.

3.7 Effective yields

The effective yield measures how a galaxys metallicity deviates from what would be expected for a closed box model of galaxy formation, i.e. a galaxy with the same gas mass fraction that had evolved without inflow or outflow of gas. A closed box galaxy evolution obeys a simple relationship between gas metallicity and the gas mass fraction. Thus, effective yields place constraints on the baryon cycle, which must have a combination of inflows and outflows of gas and metals that result in matching observed values of effective yields. The effective yield is defined as

$$y_{\rm eff} \equiv \frac{Z_{\rm gas}}{\ln\left(1/f_{\rm gas}\right)}.$$

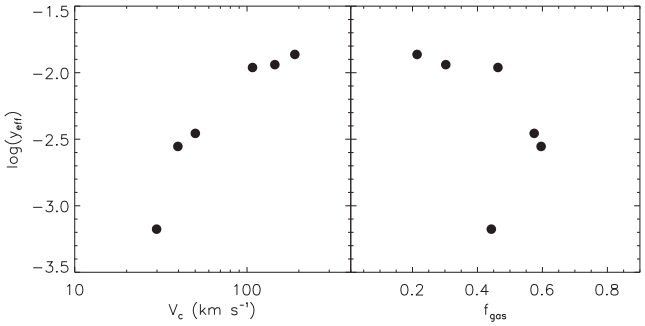

Figure 6. We plot the effective yields, $y_{\rm eff}$, as a function of rotation velocity (V_c, left-hand panel) and gas fraction ($f_{\rm gas}$, right-hand panel).

Clearly, our simulations are far from closed box models as our earlier analysis has shown, and we measure here how such deviations are reflected in the effective yields of our simulations. Fig. 6 shows the effective yields as a function of rotation velocity (V_c) and as a function of gas fraction ($f_{\rm gas}$). A flattening of the relation for galaxies with $V_c > 100$ km s^{-1} is also seen in observations (Pilyugin, Vílchez & Contini 2004), although we note an offset in effective yields between the observations and our simulations, which may be due to metallicity calibrations. The trend of effective yields with gas fraction is also similar between the simulations and observations.

3.8 Effect of metal diffusion

In Fig. 2, we overplot as dotted lines the MDFs for the two low-diffusion runs showing stars at $z = 0$ (blue dotted lines), along with the MDFs of the gas from which those stars were born, measured when the gas first accreted to the virial radius ($R_{\rm vir}$, red dotted lines), and when it first reaches the star-forming region, ($R_{\rm vir}/8$, green dotted lines). Gas with $[Z] < -5$ is shown in the plots at $[Z] = -5$. The runs with a low value for the metal diffusion coefficient ($C_{\rm Diff} = 0.01$) are consistent with the results presented previously, where we used the fiducial $C_{\rm Diff} = 0.05$, indicating that the choice of diffusion coefficient is not driving our results. We note that the complete elimination of diffusion leads to unrealistic MDF dispersions, skewness, and kurtosis (Pilkington et al. 2012).

4 DISCUSSION

The flow of gas and metals into, out of, and around galaxies comprises the baryon cycle, which ultimately is responsible for setting the characteristics observed in galaxies today. Any comprehensive theory of galaxy formation must aim for a constrained baryon cycle at its heart. Chemical evolution models attempt to do so by employing spatially resolved abundance patterns, while dynamical models attempt to match galaxy scaling relations, amongst other things. In this study, we have explored the cycle of baryons and metals within a suite of simulated galaxies that match a range of galaxy scaling relations, having been tuned to match the $M_\star$–$M_{\rm halo}$ relation (Brook et al. 2012b). Our simulations add energy only locally in star-forming regions, which drives outflows along the path of least resistance (see e.g. Brook et al. 2011). No scaling of outflows with galaxy mass or star formation rate is input by hand, nor is the direction of the outflows. Inflowing gas can penetrate and provide gas to the star-forming regions, even while outflows are occurring (e.g. Brooks et al. 2009). We have traced the infall of gas from $z = 5.5$ to the present day, to the star-forming regions of simulated galaxies that span a range in stellar mass between $M_\star = 8.9 \times 10^6$ M$_\odot$ and 3.0×10^{10} M$_\odot$. We have traced the cycle of gas through the galactic fountain for each of the galaxies, and also shown the rate at which metals are removed from the star-forming region.

We find that the universal baryon fraction accretes to the virial radius in all galaxies with halo (stellar) mass $\geq 8.3 \times 10^{10}$ (4.5×10^8) M$_\odot$. Lower mass galaxies have gas prevented from accreting by the background UV radiation field, and perhaps due to outflows, with only ∼46 per cent of the universal baryon fraction accreting to the virial radius of a galaxy of virial mass 2.2×10^{10} M$_\odot$. Significant baryonic outflows occur in each simulation, with more outflows in low-mass systems resulting in the baryon content at $z = 0$ monotonically increasing with mass, ranging from 15 to 82 per cent of the universal value in our fiducial runs. Not all the baryon baryonic content within R ever reaches the star-forming region ($R_{\rm vir}/8$): only 14 per cent of the universal value in the lowest mass case, rising to ∼80 per cent for galaxies with virial mass $\sim 3 \times 10^{11}$ M$_\odot$, while the amount of gas reaching the star-forming region in the most massive galaxy ($M_{\rm vir} = 7.6 \times 10^{11}$ M$_\odot$) is lower, 69 per cent; we speculate that this is due to shock heating at the virial radius (see Kereš et al. 2005; Brooks et al. 2009).

None of the simulated galaxies have a significant population of low-metallicity stars, with relatively narrow MDFs at all masses (n.b., see also Pilkington et al. 2012 and Calura et al. 2012). Enrichment of infalling gas occurs in three stages: (i) pre-enrichment in progenitor sub-haloes, (ii) enrichment after accretion to the virial radius but subsequent to accretion to the star-forming region, and (iii) enrichment in the star-forming region.

(i) *Pre-enrichment in progenitor sub-haloes.* In the very lowest mass halo, there is no star formation within progenitor sub-haloes, and hence only in the lowest mass halo is accreted gas not enriched by sub-haloes, polluting the IGM prior to redshift $z = 5.5$. The amount of gas pre-enriched in this manner is a strong function of galaxy mass. Accretion of pre-enriched gas goes hand in hand with the existence of an accreted halo component.

(ii) *Enrichment after accretion to the virial radius but subsequent to accretion to the star-forming region.* In all simulations, metals are ejected from the star-forming region, largely to the surrounding hot halo. As fresh gas accretes through the virial radius, it is mixed with the metals of this hot enriched halo. Further, the effect of metals is to decrease cooling times, which has an effect in selecting more metal enriched gas to preferentially accrete from the hot halo to the star-forming region. The result is that gas accreted to the star-forming region is significantly more enriched than gas accreted through the virial radius. The distribution of time-scales for gas crossing the virial radius and passing to the star-forming region is reasonably approximated by an exponential with exponent ~ -1.2 Gyr^{-1}.

(iii) *Enrichment in the star-forming region.* Low star formation efficiency in disc galaxies results in a broad distribution in the time that baryons spend between first being accreted to the star-forming region, and then subsequently forming stars. This gas may remain in the star-forming region, or cycle through the hot halo and re-accrete to the star-forming region to form stars (see Brook et al. 2012a). The result is that gas accreted to the star-forming region is significantly more enriched than gas crossing the virial radius. The distribution of time-scales between gas passing to the star-forming region and finally forming a star is reasonably approximated by an exponential with exponent ~ -4.3 Gyr^{-1}.

(iv) *Maintaining low metallicity.* Low star formation efficiency in low-mass galaxies, and a low star-to-gas ratio, means that enrichment of the ISM proceeds slowly, allowing low-mass simulated

galaxies to maintain low metallicity despite outflows being sub-solar metallicity (see Dalcanton 2007).

A significant number of stars in each galaxy form from gas that undergoes at least one *cycle through the galactic fountain*, ranging from ∼20–40 per cent, with intermediate-mass haloes ($M_{\rm vir} \sim 8 \times 10^{10}$ M$_\odot$) having the most such stars: gas in lower mass galaxies has an increasing tendency to be expelled without being re-accreted, while at the more massive end the larger potential well in higher mass galaxies means that gas is not blown as far into the hot halo. The distribution of time-scales for which gas remains within a galactic fountain is similar to that of the time taken from crossing the virial radius to arriving at the star-forming region. As we showed in Brook et al. (2012a), the distance that fountain gas reaches from the centre of the galaxy drops off exponentially. Hence, significantly more star-forming gas could be involved in smaller scale galactic fountains, particularly perpendicular to the disc, in the manner of e.g. Marinacci et al. (2011).

ACKNOWLEDGEMENTS

CBB is supported by the MICINN (Spain) through the grant AYA2009-12792. GS and AVM acknowledge support from SFB 881 (subproject A1) of the DFG. CBB acknowledges Max-Planck-Institut für Astronomie for its hospitality and financial support through the Sonderforschungsbereich SFB 881 'The Milky Way System' (subproject A1) of the German Research Foundation (DFG). We acknowledge the computational support provided by the UK's National Cosmology Supercomputer (COSMOS), as well as the theo cluster of the Max-Planck-Institut für Astronomie at the Rechenzentrum in Garching. We thank the DEISA consortium, co-funded through EU FP6 project RI-031513 and the FP7 project RI-222919, for support within the DEISA Extreme Computing Initiative, the UK's National Cosmology Super-computer (COSMOS), and the University of Central Lancashire's High Performance Computing Facility.

REFERENCES

Arrigoni M., Trager S. C., Somerville R. S., Gibson B. K., 2010, MNRAS, 402, 173
Aumer M., White S. D. M., Naab T., Scannapieco C., 2013, MNRAS, 434, 3142
Bailin J. et al., 2005, ApJ, 627, L17
Benson A. J., 2010, Phys. Rep., 495, 33
Berczik P., 1999, A&A, 348, 371
Brook C. B., Kawata D., Gibson B. K., Flynn C., 2004, MNRAS, 349, 52
Brook C. B. et al., 2011, MNRAS, 415, 1051
Brook C. B., Stinson G., Gibson B. K., Roškar R., Wadsley J., Quinn T., 2012a, MNRAS, 419, 771
Brook C. B., Stinson G., Gibson B. K., Wadsley J., Quinn T., 2012b, MNRAS, 424, 1275
Brook C. B. et al., 2012c, MNRAS, 426, 690
Brooks A. M., Governato F., Quinn T., Brook C. B., Wadsley J., 2009, ApJ, 694, 396
Calura F., Menci N., 2009, MNRAS, 400, 1347
Calura F. et al., 2012, MNRAS, 427, 1401
Chiappini C., Matteucci F., Romano D., 2001, ApJ, 554, 1044
Christensen C., Quinn T., Governato F., Stilp A., Shen S., Wadsley J., 2012, MNRAS, 425, 3058
Dalcanton J. J., 2007, ApJ, 658, 941
Dekel A., Birnboim Y., 2006, MNRAS, 368, 2
Fenner Y., Gibson B. K., 2003, Publ. Astron. Soc. Aust., 20, 189
Ferland G. J., Korista K. T., Verner D. A., Ferguson J. W., Kingdon J. B., Verner E. M., 1998, PASP, 110, 761
Few C. G., Courty S., Gibson B. K., Kawata D., Calura F., Teyssier R., 2012, MNRAS, 424, L11
Frenk C. S. et al., 1999, ApJ, 525, 554
Freyer T., Hensler G., Yorke H. W., 2006, ApJ, 638, 262
Gibson B. K., 1997, MNRAS, 290, 471
Greif T. H., Glover S. C. O., Bromm V., Klessen R. S., 2009, MNRAS, 392, 1381
Haardt F., Madau P., 1996, ApJ, 461, 20
Harfst S., Theis C., Hensler G., 2006, A&A, 449, 509
Hultman J., Pharasyn A., 1999, A&A, 347, 769
Kannan R., Macciò A. V., Pasquali A., Moster B. P., Walter F., 2012, ApJ, 746, 10
Kannan R., Stinson G. S., Macciò A. V., Brook C., Weinmann S. M., Wadsley J., Couchman H. M. P., 2014, MNRAS, 437, 3529
Katz N., 1992, ApJ, 391, 502
Kawata D., Gibson B. K., 2003, MNRAS, 340, 908
Kay S. T., Pearce F. R., Frenk C. S., Jenkins A., 2002, MNRAS, 330, 113
Kereš D., Katz N., Weinberg D. H., Davé R., 2005, MNRAS, 363, 2
Kobayashi C., Nakasato N., 2011, ApJ, 729, 16
Macciò A. V., Dutton A. A., van den Bosch F. C., 2008, MNRAS, 391, 1940
Marinacci F., Binney J., Fraternali F., Nipoti C., Ciotti L., Londrillo P., 2010, MNRAS, 404, 1464
Marinacci F., Fraternali F., Nipoti C., Binney J., Ciotti L., Londrillo P., 2011, MNRAS, 415, 1534
Marri S., White S. D. M., 2003, MNRAS, 345, 561
Martínez-Serrano F. J., Serna A., Domínguez-Tenreiro R., Mollá M., 2008, MNRAS, 388, 39
McCarthy I. G., Schaye J., Font A. S., Theuns T., Frenk C. S., Crain R. A., Dalla Vecchia C., 2012, MNRAS, 427, 379
McKee C. F., Ostriker J. P., 1977, ApJ, 218, 148
Moster B. P., Somerville R. S., Maulbetsch C., van den Bosch F. C., Macciò A. V., Naab T., Oser L., 2010, ApJ, 710, 903
Moster B. P., Naab T., White S. D. M., 2013, MNRAS, 428, 3121
Nomoto K., Iwamoto K., Nakasato N., Thielemann F.-K., Brachwitz F., Tsujimoto T., Kubo Y., Kishimoto N., 1997, Nucl. Phys. A, 621, 467
Pearce F. R., Jenkins A., Frenk C. S., White S. D. M., Thomas P. A., Couchman H. M. P., Peacock J. A., Efstathiou G., 2001, MNRAS, 326, 649
Pelupessy F. I., Papadopoulos P. P., van der Werf P., 2006, ApJ, 645, 1024
Pilkington K. et al., 2011, MNRAS, 417, 2891
Pilkington K. et al., 2012, MNRAS, 425, 969
Pilyugin L. S., Vílchez J. M., Contini T., 2004, A&A, 425, 849
Prochaska J. X., Weiner B., Chen H.-W., Mulchaey J., Cooksey K., 2011, ApJ, 740, 91
Renda A., Gibson B. K., Mouhcine M., Ibata R. A., Kawata D., Flynn C., Brook C. B., 2005, MNRAS, 363, L16
Robertson B. E., Kravtsov A. V., 2008, ApJ, 680, 1083
Samland M., Gerhard O. E., 2003, A&A, 399, 961
Samland M., Hensler G., Theis C., 1997, ApJ, 476, 544
Sawala T., Scannapieco C., Maio U., White S., 2010, MNRAS, 402, 1599
Scannapieco C., Tissera P. B., White S. D. M., Springel V., 2006, MNRAS, 371, 1125
Scannapieco C. et al., 2012, MNRAS, 423, 1726
Semelin B., Combes F., 2002, A&A, 388, 826
Shen S., Wadsley J., Stinson G., 2010, MNRAS, 407, 1581
Smagorinsky J., 1963, Mon. Weather Rev., 91, 99
Spergel D. N. et al., 2007, ApJS, 170, 377
Springel V., Hernquist L., 2003, MNRAS, 339, 312
Springel V. et al., 2008, MNRAS, 391, 1685
Steinmetz M., Mueller E., 1994, A&A, 281, L97
Stinson G., Seth A., Katz N., Wadsley J., Governato F., Quinn T., 2006, MNRAS, 373, 1074
Stinson G. S., Bailin J., Couchman H., Wadsley J., Shen S., Nickerson S., Brook C., Quinn T., 2010, MNRAS, 408, 812
Stinson G. S. et al., 2012, MNRAS, 425, 1270
Stinson G. S. et al., 2013a, MNRAS, 436, 625
Stinson G. S., Brook C., Macciò A. V., Wadsley J., Quinn T. R., Couchman H. M. P., 2013b, MNRAS, 428, 129

Thacker R. J., Couchman H. M. P., 2001, ApJ, 555, L17
Timmes F. X., Woosley S. E., Weaver T. A., 1995, ApJS, 98, 617
Tissera P. B., White S. D. M., Scannapieco C., 2012, MNRAS, 420, 255
Torres G., 2010, AJ, 140, 1158
Tumlinson J. et al., 2011, Science, 334, 948
van den Hoek L. B., Groenewegen M. A. T., 1997, A&AS, 123, 305
Wadsley J. W., Stadel J., Quinn T., 2004, New Astron., 9, 137
Wadsley J. W., Veeravalli G., Couchman H. M. P., 2008, MNRAS, 387, 427
Woosley S. E., Weaver T. A., 1995, ApJS, 101, 181

This paper has been typeset from a TEX/LATEX file prepared by the author.